

Pathfinder – Navigating and Analyzing Chemical Reaction Networks with an Efficient Graph-based Approach

Paul L. Türtscher¹ and Markus Reiher²

Laboratory of Physical Chemistry, ETH Zurich,
Vladimir-Prelog-Weg 2, 8093 Zurich, Switzerland

September 08, 2022

While the field of first-principles explorations into chemical reaction space has been continuously growing, the development of strategies for analyzing resulting chemical reaction networks (CRNs) is lagging behind. A CRN consists of compounds linked by reactions. Analyzing how these compounds are transformed into one another based on kinetic modelling is a non-trivial task. Here, we present the graph-optimization-driven algorithm and program PATHFINDER to allow for such an analysis of a CRN. By encoding the reactions of a CRN as a graph consisting of compound and reaction nodes and adding information about activation barriers as well as required reagents to the edges of the graph yields a complete graph-theoretical representation of the CRN. Since the probabilities of the formation of compounds depend on the starting conditions, the consumption of any compound during a reaction must be accounted for to reflect the availability of reagents. To account for this, we introduce compound costs to reflect compound availability. We first illustrate the working principle on an abstract small CRN. Afterwards, PATHFINDER is demonstrated at the example of the disproportionation of iodine with water and the comproportionation of iodic acid and hydrogen iodide. Both processes are analyzed within the same CRN which we construct with our autonomous first-principles CRN exploration software CHEMOTON [arXiv:2202.13011] guided by PATHFINDER.

¹ORCID: 0000-0002-7021-5643

²Corresponding author; e-mail: markus.reiher@phys.chem.ethz.ch; ORCID: 0000-0002-9508-1565

1 Introduction

Chemical reaction networks (CRNs) are molecular transformation webs with compounds connected by chemical reactions. Various computational strategies have been reported in the literature to explore chemical reaction space with quantum chemical methods and map out such CRNs.^{1–7} These advanced exploration techniques make CRNs with increasing numbers of compounds and reactions accessible. Alongside, the challenge of analyzing such large and interwoven networks is slowly surfacing. Due to the high connectivity of a CRN, it is non-trivial to assess how specific compounds are formed. This complexity is due to the fact that a compound of interest is likely formed through various reaction channels, each channel consisting of a sequence of reactions. This multitude of options raises the question which channel or path is most frequently followed.

Microkinetic modeling^{8–12} to approach this problem may not be viable, if very many coupled ordinary differential equations that describe all concentration changes are to be considered and span largely different time scales. Then, the time required to simulate concentration fluxes through such a CRN can be exceedingly long. Moreover, the sequence of reactions which form a compound in question is not directly retrieved.

However, the CRN can be represented as a graph (see, e.g., Refs. 5,13,14). A graph is an obvious representation as all compounds are interconnected via reactions in a CRN. For instance, a compound can be a reagent of one and the product of another reaction. Once the graph is established, it can be analyzed to identify the shortest simple path between two compounds. A shortest simple path is of minimal length with the lowest possible sum of the edge weights and nodes that are only visited once. Shortest path is to be understood as the most efficient path, not necessarily the path with the least number of steps (reactions). In the context of this work, the shortest path is the most probable sequence of reactions from a source node to a target node expressed by the lowest possible sum of edge weights.

Determining the most probable sequence of reactions between two compounds is a shortest path problem. Extracting such paths in terms of a likelihood for reaction mechanisms and synthesis routes has been accomplished based on depth-first algorithms.^{15–17} A drawback of these approaches is that they are specifically tailored solutions for a specially constructed and pruned CRN. For example, the stoichiometric requirements of a reaction are not considered or circumvented by construction. This makes these approaches not generally applicable and insufficient for larger networks.

Persson and co-workers employed efficient algorithms from graph theory to identify paths in a CRN.^{18,19} This allowed them to find one or multiple shortest paths with Dijkstra's²⁰ and Yen's²¹ algorithms in CRNs containing only three types of reac-

tions and thermodynamic information. These authors extended their approach to problems of solid-state material synthesis where the CRN consists of phases instead of compounds.²²

For large CRNs, a graph-based approach identifying connections between compounds is computationally too demanding and requires a Monte Carlo-based strategy.²³ Such an approach has been exploited to study the formation of solid-electrode interfaces.²⁴ However, the challenge of analyzing a CRN is rooted in its construction. The construction of the CRN in Ref. 23 relies on enumeration and filtering of all stoichiometrically valid reactions based on a set of compounds. The compounds of a set have the same composition in terms of their atoms (identical molecular formula). Reactions are then generated by choosing all possible combinations of two compounds in each set, each compound for one side of the reaction. During construction of a CRN it is not validated whether the two sides of a reaction are actually connected through a transition state. Each set consisting of m compounds results initially in $m!/(m - 2)!$ reactions. For instance, a set with 10 compounds yields 90 reactions, a set with 50 compounds already 2450 reactions. By applying filters to the initial reactions, the number of reactions decreases. Still, the underlying combinatorial approach in Ref. 23 produced a CRN with about 86000000 reactions. By contrast, the exploration strategy developed in our group^{25–27} explores CRNs through *ab initio* calculations. Accordingly, all reactions discovered connect compounds at least via one elementary step with a transition state. Hence, a combinatorial approach, which assumes that all reactions are possible followed by a subsequent filtering, is avoided.

In this work, we present a unique graph-based approach to represent any multi-reactant reaction in a CRN including kinetic and stoichiometric information that then allows for the identification shortest paths between any two compounds. The term reaction is to be understood in the most general sense in this context; it can involve catalysts, solvents, and surfaces. Building the graph is neither affected by the type of reactant nor does it require a tailored template to represent it. The stoichiometric requirements encoded in the graph carry information about which reagents are consumed when one compound node is transformed into another one. Including the stoichiometry alongside kinetic information for a specific reaction in the graph is crucial for the assessment of how costly it is to traverse the network through the corresponding reaction node in the graph, since it is, in addition to the reaction barrier, important to know whether the necessary reagents are available at all. Then, the graph representation allows to query the network for the shortest simple path between any two nodes employing efficient pathfinding algorithms. The analysis of a CRN based on given starting conditions returns a ranking of its compounds corresponding to the probabilities of encountering them. Based on such a ranking, a running CRN exploration can be steered on the fly and, therefore, focused on kinetically relevant areas of the network.

We introduce our PATHFINDER algorithm in Sec. 2, apply it to an abstract network taken from the literature¹⁸ in Sec. 4.1, and illustrate its predictive power for the disproportionation of I_2 with H_2O ,^{28–31} for which we provide a new CRN of gas-phase reactions. In this case, PATHFINDER fulfills two tasks: guiding the exploration and analyzing the final CRN in order to allow for a comparison of paths from I_2 to iodic acid, HIO_3 , and vice versa.

2 Theory

We adopt the notation for first-principles CRNs from Ref. 27: A chemical *structure* is given by a fixed atom type and number, fixed nuclear positions, a fixed number of electrons and total spin. It therefore represents a specific point on the Born–Oppenheimer potential energy surface. By contrast, a *compound* denotes a set of chemical structures with the same atom types and number, charge, spin, stereochemistry, and, most importantly, connectivity. For instance, the boat and chair conformations of cyclohexane, clearly different structures, are considered the same compound. A *reaction* is defined as a collection of elementary steps that connect compounds, whereas an elementary step within a reaction connects structures of these compounds by different transition states (TSs).

Given a CRN defined for a set of compounds and reactions, one is interested in the kinetically most likely sequence of reactions within this CRN connecting two given compounds. We dissect the search for such sequences into three steps: First, a graph network is built from chemical reactions. Second, a cost measure for the probability of a reactant being available for a reaction is evaluated. We refer to this cost as *compound cost*. Third, the graph network is updated with the information about the costs of the reactants. These three steps are sketched in Fig. 1.

The compound costs will depend on which compounds are available with some probability at the start. The probabilities can be derived from compound concentration ratios of concentrations, pressure or volume. The starting conditions can be deliberately chosen. Given the costs for at least one reactant, the costs for all other reactants follow (for details see below).

The resulting graph representation of the CRN can be queried for sequences of reactions, named paths in this context. A typical query asks for the shortest paths starting from one starting compound to a compound of interest. The obtained paths between two compounds are ordered by their path length which is linked to their probability.

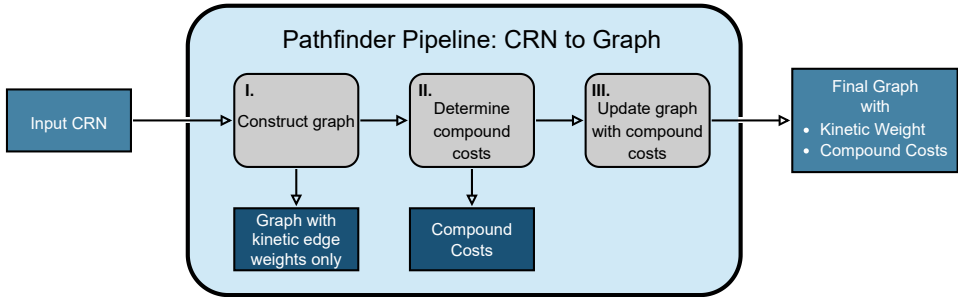


Figure 1: Schematic representation of the three steps necessary to convert a CRN to a graph containing kinetic as well as stoichiometric information. Input and output are colored in blue, operations sequentially performed on the input in gray and the intermediate objects in dark blue.

2.1 Graph-theoretical Representation of Reactions

In a given list of reactions (see Sec. 3 for details on their exploration), each reaction corresponds to a subgraph of the graph representation of the whole CRN. Therefore, the whole CRN is built by sequentially adding (parts) of such a subgraph. Two 'reaction nodes' represent the TS structure of the reaction with the additional information from which side of the reaction the reactants approached the TS. Accordingly, they are labeled as 'left hand side' (LHS) reaction node in case one starts from the reactants and 'right hand side' (RHS) reaction node in case one starts from the products, although such an assignment is to a certain degree arbitrary and solely serves the purpose to allow for directional distinction. In our context, the way a reaction is formulated depends on how our reactions exploration software CHEMOTON stored the reaction in the database. The assignment itself does not alter the graph as reaction nodes are only connected to reactants and products of a reaction.

Next, the reactants and products will be added to the network as nodes if they have not already been included in the CRN yet. The added nodes are connected with directional edges where reactants are linked to the LHS reaction node and the LHS reaction node then to the products. In turn, the products are connected to the RHS reaction node and the RHS reaction node then to the reactants. The edges are directional to enforce the traversal from one side to the other as shown in Fig. 2.

Furthermore, an edge contains an edge weight (measuring how costly it is to traverse this edge), a list of required compounds, and the sum over the compound costs of the reagents in the required compounds list. These terms are explained in detail in Sec. 2.2. A schematic representation of this architecture is shown in Fig. 2. This architecture allows to encode any kind of reaction from the CRN in the graph, regardless of the number of involved reactants or emerging products.

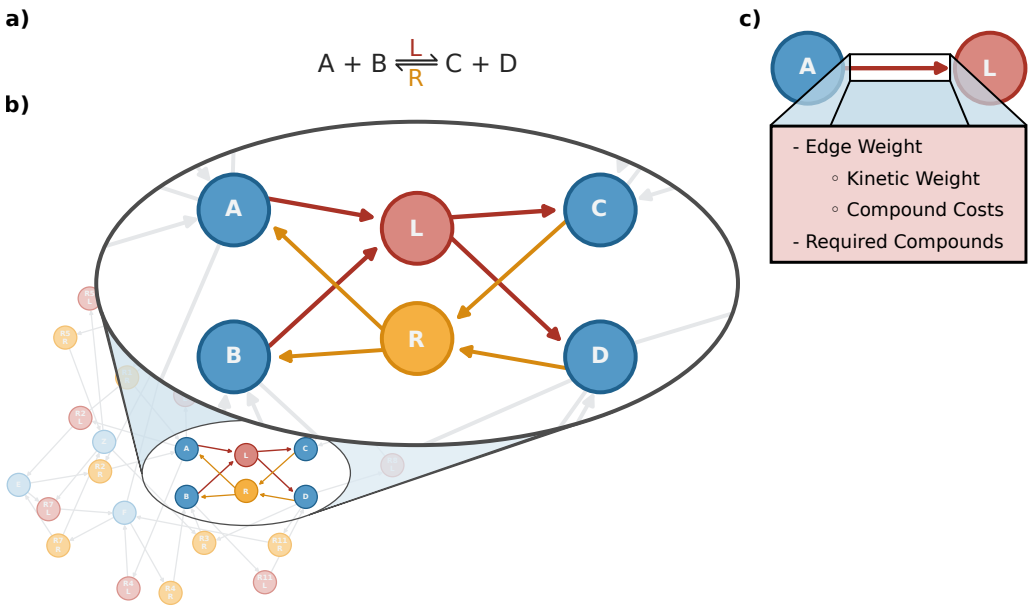


Figure 2: **a)** Prototypical chemical reaction in a CRN. **b)** The same reaction in the CRN represented as a graph. Compounds are depicted as blue nodes, the reaction node 'L' indicating the approach of the reactants toward the TS from the left hand side as a red node, and the reaction node 'R' indicating approaching the TS from the right hand side as an orange node. **c)** Properties stored in the edge from a compound node to a reaction node. Addends of the edge weight for the final graph, the kinetic weight and the compound costs. In this case, the required compound in **c)** is B.

The size of the graph measured in terms of the numbers of nodes and edges grows with each reaction added. At least two nodes will be added to the graph per reaction, if all occurring compounds are already part of the graph. The maximum number of added nodes per reaction is given by two plus the number of compounds of the reaction which are yet to be included in the existing graph. Concerning the number of edges per reaction, the reaction nodes have incoming edges equal to the reacting compounds and outgoing edges equal to the number of product compounds. Hence, the number of edges per added reaction is the number of compounds of the reaction times two.

The problem at hand is a shortest path problem, hence a long edge indicates that the traversal via this edge is unfavorable. The length of an edge, i.e., the edge weight, is added as information to the edge when connecting the nodes as shown in Fig. 2. Furthermore, the list of compounds required for this reaction is added. This list will be key for the second step of our algorithm in order to determine the costs for consuming compounds during a shortest path search. In the final step of

the PATHFINDER pipeline to convert a CRN to a graph containing kinetic as well as stoichiometric information, the sum over all compound costs of the compounds in the list of required compounds is written to the edge as compound costs. This sum is then added to the existing edge weight and allows us to consider the cost of consuming the required compounds of each reaction when querying the resulting graph directly.

2.2 Kinetic Weights

The initial weights for edges from compound nodes to reaction nodes, $C/D \rightarrow R$ and $A/B \rightarrow L$, are based on the free activation energies, ΔG_{TS-LHS} or ΔG_{TS-RHS} , of the reaction. The free activation energies themselves are not suitable as edge weights as they are not reflecting the exponential character considering kinetics. Hence, the free activation energy is turned into a rate constant. The rate constant k_i , denoting k_{LHS} and k_{RHS} of reaction i in a simplified notation, can be obtained according to Eyring's absolute rate theory,

$$k_i = \frac{k_B T}{h} \exp\left(-\frac{\Delta G_{TS-i}}{RT}\right), \quad (1)$$

where T is the temperature, k_B Boltzmann's constant, h Planck's constant, and R the ideal gas constant (accordingly, the energy difference is then to be given in energy units per mole substance).

Note that the edge weights from reaction nodes to product nodes (e.g., $L \rightarrow C/D$ and $R \rightarrow A/B$ in Fig. 2) are set to zero throughout this work as the reaction progress from the TS to the product is energetically downhill in an elementary step.

Since rate constants are not directly suitable as edge weights in a shortest path problem (owing to the anticorrelation that large rates would correspond to short paths), we consider a few additional steps. Moreover, we note that rate constants can cover a large range of magnitudes, e.g., from $1 \times 10^{-12} \text{ s}^{-1}$ to $1 \times 10^{12} \text{ s}^{-1}$. Hence, when adding edge weights, very small weights will hardly affect the total sum if a large edge weight is already part of the path. A large range of weights is therefore disadvantageous for the rigorous assessment of the shortest path problem, because paths going via different reactions besides one with a large edge weight would end up with the same length.

The correspondence of low reaction barrier to low edge weight as required for the shortest path problem could be solved by taking the inverse of k_i , $1/k_i$ [s]. A low barrier would then correspond to a short time (low weight) to traverse an edge, but the problem of a large spread for the edge weights remains. Hence, to minimize the spread we normalize each rate constant k_i by the sum over all rate constants in the

CRN to obtain the relative rate constant p_i with

$$p_i = \frac{k_i}{\sum_l^{\text{all } k_{\text{LHS}}} k_l + \sum_r^{\text{all } k_{\text{RHS}}} k_r}. \quad (2)$$

This definition can be rationalized by recalling that the rate v_i of a reaction i is given by

$$v_i = k_i \prod_j^{\text{reactants}} c_j, \quad (3)$$

where c_j are the (time-dependent) concentrations of the reactants. If all concentrations of all reactants are considered equal to 1 mol/l and time-independent, the rate v_i will be simply given by the rate constant k_i . This assumption may also be understood literally as a short-time approximation to a case, in which all compounds (also the stable intermediates usually produced only later in the course of a reaction starting from one or two reactants) are already available right from the start and at a concentration of 1 mol/l. This assumption is necessary to avoid explicit propagation of concentration flows through microkinetic modeling, because this would be far too time consuming. Under this short-time all-species-present assumption, the relative rate constant p_i in a CRN is equal to the relative rate and can be interpreted as a measure for the likelihood or probability of the reaction step i to occur relative to all other reaction steps in the CRN. The probability of a sequence of reaction steps is the product of the individual reaction probabilities, assuming that each reaction is independent of all other reactions (cf. Eq. (2)).

Since a high probability of a path corresponds to a high likelihood that the path's product is formed through this reaction sequence, it still contradicts the requirement of a low edge weight for a favorable shortest path. Therefore, we introduce a cost function $f(p_i)$,

$$f(p_i) = -\ln(p_i) = \ln\left(\frac{1}{p_i}\right) \equiv w_i, \quad (4)$$

which possesses the salient feature that it results in weights w_i which are additive to yield a total weight (instead of multiplicative probabilities that yield a total probability):

$$\begin{aligned} w_{tot} &= w_1 + w_2 + w_3 + \dots + w_i \\ &= \ln\left(\frac{1}{p_1}\right) + \ln\left(\frac{1}{p_2}\right) + \ln\left(\frac{1}{p_3}\right) + \dots + \ln\left(\frac{1}{p_i}\right) \\ &= \ln\left(\frac{1}{p_1} \frac{1}{p_2} \frac{1}{p_3} \dots \frac{1}{p_i}\right) = \ln\left(\frac{1}{p_{tot}}\right), \end{aligned} \quad (5)$$

where w_{tot} is the total weight or length of a path and p_{tot} its total probability. Note in this context that shortest-path algorithms typically sum over the weight of edges to determine a shortest path.³² The edge weights w_i are given in arbitrary units abbreviated as a.u. throughout this work. We call these weights derived from activation barriers entering our definition of the cost function *kinetic weights*.

2.3 Compound Costs

If a compound can only be reached through reactions with high barriers, it may be unlikely that it can be formed under certain reaction conditions. This fact must be considered when consuming the compound in another reaction, for which it will simply not be available. Hence, querying a CRN which encodes only the kinetic weights as edge weights would lack information about the stoichiometric requirement that compound C produced from compound A requires compound B as reactant in our example in Figure 2. To take this into account, we introduce a *compound cost* c_i for every compound i in the graph. For one edge from a compound node to a reaction node, the additional costs caused by consuming the required compounds are encoded as the sum over the compound costs of all compounds required for a reaction. This sum of costs added to the edge weight w_i ,

$$w'_i = w_i + \sum_l^{\text{required compounds}} c_l, \quad (6)$$

results in w'_i . w'_i of an edge i is calculated on-the-fly when searching for the shortest path for determining the compound costs, the graph itself is not altered yet. A compound cost c_i is defined as the shortest path from one of the starting compounds to the compound i , considering the kinetic weight and the sum of compound costs of the required compounds,

$$\begin{aligned} c_i &= c_{\text{start}} + \sum_j^{\substack{\rightarrow \text{R/L edges} \\ \text{in shortest path}}} w'_j \\ &= c_{\text{start}} + \sum_j^{\substack{\rightarrow \text{R/L edges} \\ \text{in shortest path}}} \left(w_j + \sum_l^{\text{required compounds}} c_l \right), \end{aligned} \quad (7)$$

where c_{start} corresponds to the compound cost of the path's starting compound. As the determination of the compound cost c_i requires other compound costs, the costs must be determined iteratively, given the CRN and the starting conditions, to

obtain self-consistent compound costs, $c_{i,sc}$. Hence, Eq. 7 is re-written as

$$c_{i,n} = c_{\text{start}} + \sum_j^{\rightarrow \text{R/L edges in shortest path}} \left(w_j + \sum_l^{\text{required compounds}} c_{l,n-1} \right), \quad (8)$$

where n indicates the current iteration step.

The algorithm to determine the compound costs is outlined in Fig. 3. To determine the required compound costs for all compounds in the CRN, we define starting conditions by assigning compound costs to selected starting compounds. These compounds are those compounds available at the initialization of a reactive system under consideration, similar to reactants present in a flask at the beginning of a reaction in an experiment.

When calculating costs of all other compounds, denoted here as 'unknown compounds', the results will depend on the chosen starting compounds and their costs. Hence, one can end up with different compound costs by choosing different starting conditions. Before starting the first iteration, all unknown compounds are assigned an infinite positive cost,

$$c_{i,0} = \begin{cases} 0 \leq x < \infty, & i \in \text{starting compounds} \\ \infty, & \text{otherwise.} \end{cases} \quad (9)$$

and with the compound costs for the starting compounds, all compounds have a $c_{i,0}$ assigned. Then, the algorithm starts an outer loop over the set of starting compounds, the first iteration ($n = 1$), and an inner loop over all unknown compounds.

The shortest path from a starting compound to a target compound is found with Dijkstra's algorithm.²⁰ In principle, any other algorithm to determine the shortest path between the two compounds could be employed.

If compounds of infinite costs would need to be consumed along the shortest path to a target compound, the algorithm stops any further analysis of this path and instead continues to find a path for the next target compound. If the shortest path does not require consumption of compounds with infinite cost, the compound cost of the starting compound is added to the current total path weight (see Eq. 8) resulting in $c'_{i,n}$ for the target compound i . The current total weight $c'_{i,n}$ is calculated as stated in Eq. 8. Employing compound costs of the previous iteration ensures that the order of compounds analyzed is not relevant during an iteration over all compounds. The current total weight $c'_{i,n}$ for the target compound i will be defined as $c_{i,n} := c'_{i,n}$ if $c'_{i,n} < c_{i,n-1}$ and, if $c_{i,n}$ has been previously defined, $c'_{i,n} < c_{i,n}$.

After iterating over all starting compounds, the compound costs of the current iteration are completed with $c'_{i,n-1}$ for all compounds where the condition $c'_{i,n} < c_{i,n-1}$

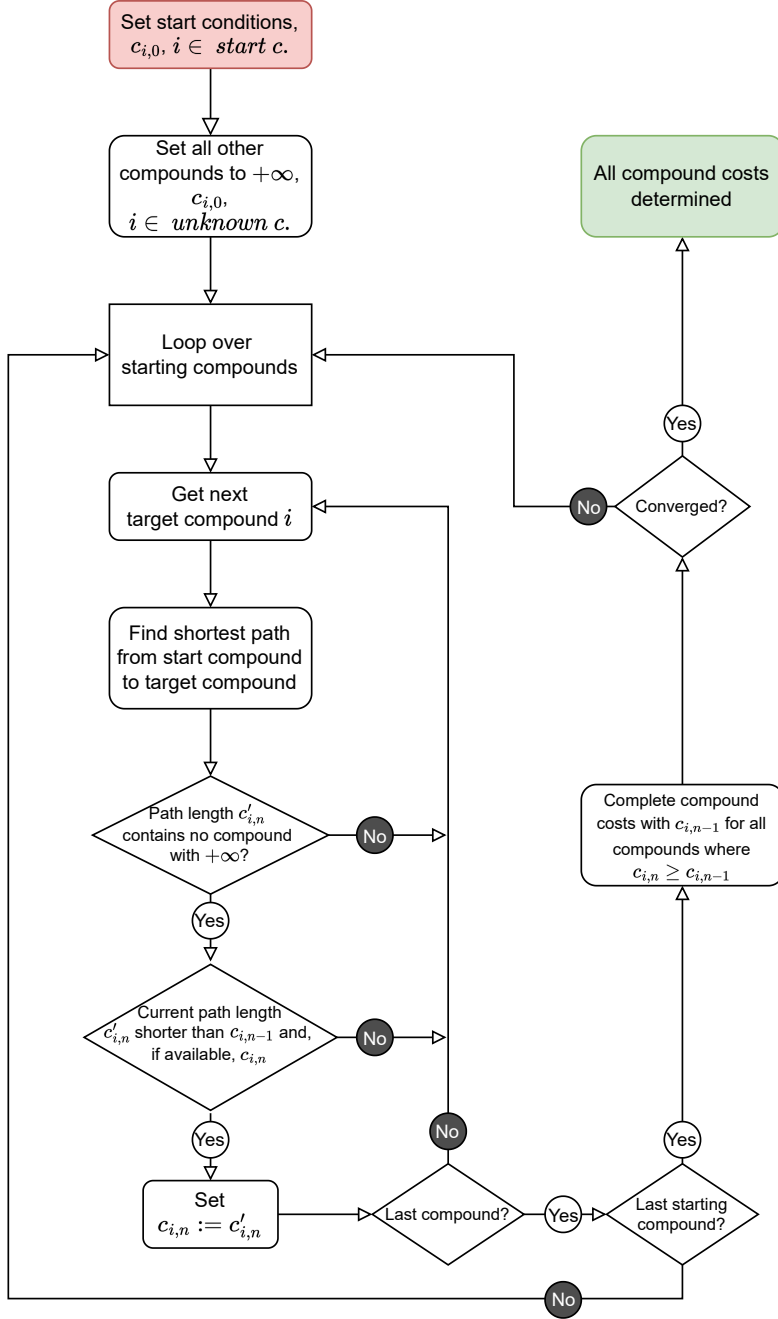


Figure 3: Flow chart of the algorithm to determine the compound costs in a CRN graph.

was not met. This guarantees that all compounds have a cost assigned for a possible subsequent iteration step.

Finally, it is inquired whether the costs of the compounds have converged. Convergence will be achieved if all compounds have costs smaller than the assigned infinite

value and self-consistency in the costs is reached. Self-consistency is achieved if none of the compound costs were altered in the current iteration. The loop over the starting compounds is restarted until convergence. Upon convergence, all compounds have costs assigned characterizing the length of the shortest paths from a starting compound to them and we achieve convergence, i.e.,

$$c_{i,sc} := c_{i,n} \quad (10)$$

for all compounds $i, i \in \text{unknown compounds}$.

2.4 Update Graph to Include Compound Costs in Edge Weights

With the self-consistent compound costs determined, the edges and edge weights of the graph are updated. The sum of all compound costs C_i in an edges i

$$C_i = \sum_l^{\text{required compounds}} c_{l,sc}, \quad (11)$$

is stored in the corresponding compound-costs array. C_i is then added to the edge weight w_i ,

$$w_i^f = w_i + C_i, \quad (12)$$

resulting in w_i^f which is set as the edge weight of an edge from a compound node to a reaction node (compare Fig. 2c). Consequently, the edge weight holds the kinetic information as well as the information about the accessibility of the required compounds to traverse along this edge. In this way, final edge weights in the updated graph of a CRN depend on the chosen starting conditions. By altering the starting conditions of the identical CRN, graphs with different compound costs and, consequently, different edge weights can be obtained and compared.

The graph can now be queried from any source compound to any other target compound. The shortest paths between these two nodes are determined with Yen's algorithm,²¹ which in turn is based on Dijkstra's algorithm.²⁰ The returned path consists of a sequence of compound nodes and reaction nodes and the total weight or length of the path.

3 Computational Methodology

PATHFINDER implements our approach described so far in PYTHON3. It can process network data produced by our autonomous first-principles CRN exploration software

CHEMOTON.^{27,33} The CRN’s graph is represented and the shortest path is queried through the PYTHON3 package NETWORKX.³² Parts of PATHFINDER are already available open source and free of charge in SCINE HERON³⁴ and the full functionality will be made available with future releases of CHEMOTON³⁵ and SCINE HERON.³⁶ All data presented in this work were generated with this SCINE software framework,³⁷ stored in and processed from the SCINE database.³⁸ All calculations were handled by SCINE PUFFIN instances.^{27,39} These instances interface SCINE READUCT,^{40,41} MOLASSEMBLER^{42,43} and the SCINE UTILITIES.⁴⁴ New elementary steps were found by elementary-step trials with SCINE CHEMOTON.³³ Details on the options for the generating the trials are stated in the supporting informations (SI). To generate transition state guesses, the Newton Trajectory Algorithm 1 (NT1)²⁷ was selected. Detailed settings for all parts of the NT1 job are listed in the SI. CHEMOTON assigns newly found elementary steps to reactions as well as new structures to compounds in an automatic fashion based on their definitions outlined in Sec. 2, thereby constructing the CRN. We refer the interested reader to Ref. 27 for a detailed description of the underlying algorithms.

For the construction of a chemical reaction network, a list of reactions is required. The elementary steps of each reaction must consist of reactant structures and assigned energies as well as product structures and assigned energies. Both sets are then supplemented with (free) activation energies for both reaction directions. This information is easily accessible from an explored CRN when stored in a database.²⁷ In our framework, a reaction consists of multiple elementary steps, where each elementary step features its own barrier height. Hence, each reaction is assigned a range of activation energies, of which the lowest indicate those elementary steps with highest probability to dominate the reaction’s mechanism. The obtained list of reactions can be subjected to additional filter criteria. For instance, only reactions with barriers in both direction below a given threshold may be forwarded to the ‘CRN to Graph’ pipeline of PATHFINDER (cf. Fig.1). The CRN generated with CHEMOTON here and the graph representation obtained with PATHFINDER will be made available on Zenodo. To produce the raw data for the CRN, electronic-structure Kohn-Sham density functional theory calculations were automatically launched by PUFFIN were carried out with the program package TURBOMOLE (V7.4.1),⁴⁵ applying the PBE functional^{46,47} with a def2-SVPD basis set^{48–50} and semi-classical D3 dispersion corrections.⁵¹ All calculations were performed without imposing any point-group symmetry, i.e., in point group C₁. We note that almost all activation barriers were calculated as Gibbs free energy differences of transition state structures and stable intermediates, assuming the rigid-rotor/harmonic-oscillator/particle-in-a-box model at a temperature of 298.15 K and a pressure of 1 atm under ideal gas conditions. The Hessian matrix required for the vibrational analysis in the harmonic-oscillator model was calculated analytically with TURBOMOLE. There are 17 exceptions where only

electronic energy differences were available because of monoatomic molecules on either reactant or product site of the reaction. For each reaction, only the free activation energies of the elementary step with the TS with the lowest free energy are considered as the key representative for a reaction under consideration. However, it is also possible to employ a (weighted) average over all (free) activation energies.

4 Results and Discussion

4.1 Synthetic Example

We first demonstrate the working principle of PATHFINDER with the example of a CRN consisting of the following 10 reactions:

$A \rightleftharpoons B$	$w_{R1} = 6$	(R1)
$A \rightleftharpoons D + E$	$w_{R2} = 1$	(R2)
$A \rightleftharpoons Y + Z$	$w_{R3} = 2$	(R3)
$A \rightleftharpoons F$	$w_{R4} = 4$	(R4)
$Z \rightleftharpoons B$	$w_{R5} = 3$	(R5)
$B + D \rightleftharpoons K$	$w_{R6} = 1$	(R6)
$E + Z \rightleftharpoons F$	$w_{R7} = 2$	(R7)
$Y + Y \rightleftharpoons K$	$w_{R8} = 4$	(R8)
$B + B \rightleftharpoons H$	$w_{R9} = 3$	(R9)
$F + K \rightleftharpoons H$	$w_{R10} = 1$	(R10)

The reactions R1–R10 and the initial edge weights in forward and backward directions were taken from Blau et al.¹⁸ Given only compound A at the start of the reaction, we query the shortest path from A to H. At first glance, the shortest path in terms of the number of reactions is R1 yielding compound B followed by R9 producing compound H directly from two equivalents of compound B. However, the weight via R1 is quite high and hence a path along this reaction will be unlikely. The visual representation of the iterative determination of all compound costs (compare Fig.3) is given in Fig.4.

In the first iteration step of the PATHFINDER algorithm, the compound costs (compare Fig.4) of products from reactions only directly consuming the starting compound A as a reagent were assigned. Compounds H and K were not accessible in

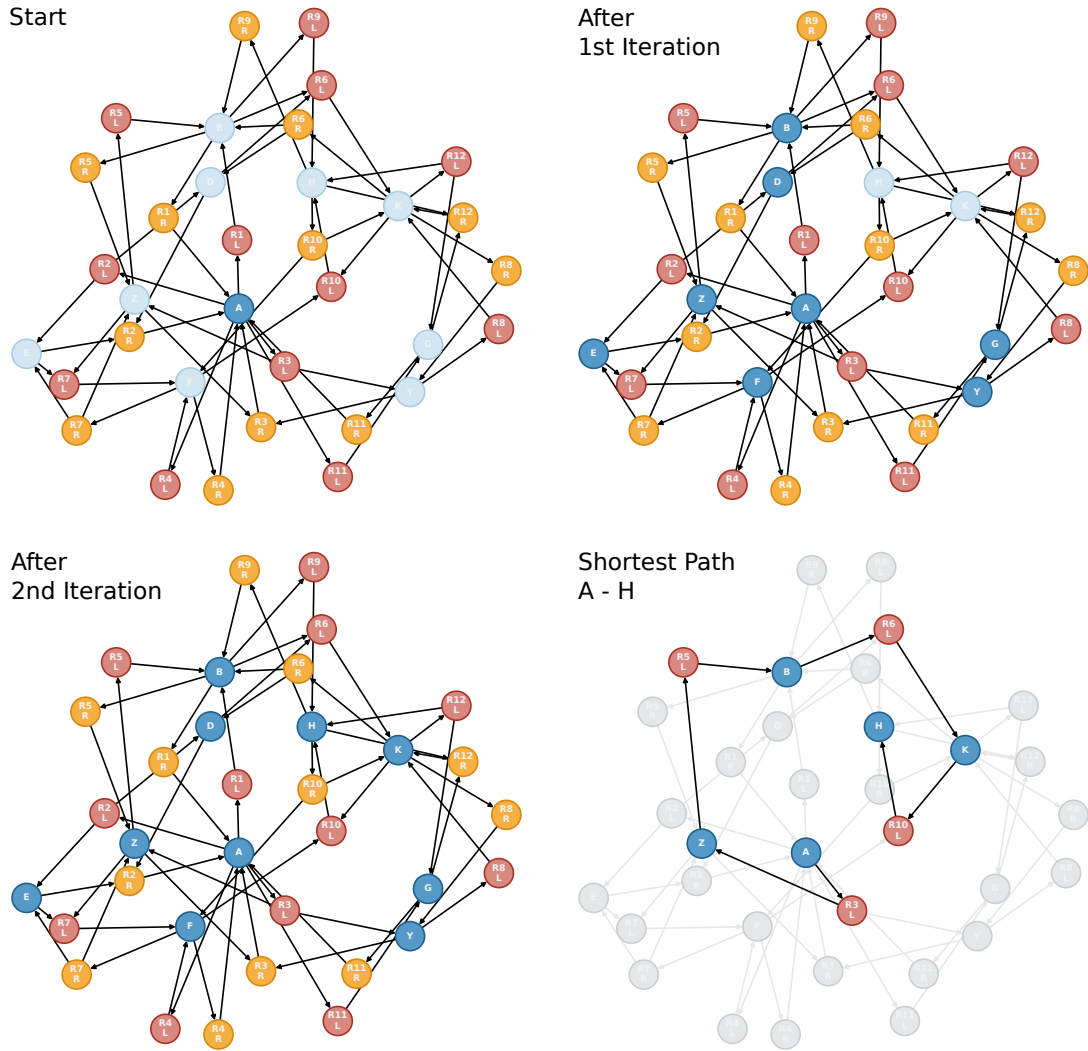


Figure 4: Determination of the compound costs in a model CRN of 10 reactions. Compounds with assigned costs are shown in dark blue, compounds without in light blue. LHS reaction nodes are represented in red, RHS reaction nodes in orange. At the start, only the starting compound has a compound cost (top left). After the first iteration step, all compounds, apart from compounds K and H, have a compound cost assigned (top right). After the second iteration step, also compounds K and H carry compound costs (bottom left). Not depicted here is the final third iteration step, which is performed to control if new paths including K and/or H can be found. Bottom right: the shortest path from compound A to compound H is highlighted, all other nodes and edges are shown in gray.

the first iteration as reactions forming those two require reactants not initially available. In the second iteration step, valid paths to the two remaining compounds were found such that all compounds ultimately had a cost assigned. In the third and last step, it was checked whether the availability of the two new compounds lowered any

of the previously determined compound costs, which turned out to be not the case in this example.

To probe internal consistency of the compound cost determination, we added two reactions, R11 and R12, to the CRN (R1–R10):



Although R11 is quite costly, the only path to G was through this reaction in the first iteration step. As compounds L and H were only encountered in the second iteration step, the compound cost of G could only be reduced when the costs for the other two compounds were determined. This was accomplished in the third iteration step which caused PATHFINDER to iterate a fourth time. In the fourth step, it was probed whether the new compound cost of G caused any other compound costs to change.

4.2 Exploration of I_2 with H_2O

We now turn to a CRN produced with our CHEMOTON exploration software. The CHEMOTON driven first-principles exploration was guided *on-the-fly* by the ranking of compounds provided by PATHFINDER. The initial starting reagents were chosen to be iodine and water only. I_2 was assigned a compound cost of 1.0 a.u., H_2O a compound cost of 0.45 a.u.. This corresponded approximately to a ratio of $I_2 : H_2O$ of 1 : 2 and hence to a probability of 36% ($e^{-1.0}$) for I_2 and 64% ($e^{-0.45}$) for H_2O at the start of the reaction. During the guided exploration, a total of 49710 structures as well as 15519 elementary steps from 100997 elementary-step trials were found by CHEMOTON.

The structures and elementary steps found were aggregated into a total of 1157 compounds and 4540 reactions. Given the simplicity and small size of our starting molecules, this number of compounds is astonishing. However, as an iodine atom is able to form up to seven bonds, quite similar to transition metals, the first coordination sphere of iodine can vary significantly. For instance, orthoperiodic acid and diperiodate species coordinate six oxygen atoms per iodine atom.⁵² Accordingly, the surprisingly large number of compounds is produced by a varying number of atoms bound to I and by their different types (and environments) – similar to ligands in transition metal complexes. In addition, stereoisomers (cis/trans, fac/mer) come into play. As two iodine atoms can bind either directly or be bonded via a bridg-

ing oxygen atom, the number of theoretically possible compounds grows even more. These compounds might be high in energy and, hence, meta-stable; nevertheless, they are minima on the investigated potential energy surface. However, we emphasize that all species found in our network are, by construction, uncharged species in the gas phase. Hence, important solvation effects are absent, and therefore, charged species are not present.

$\text{H}-\text{O}-\text{H}$	$\text{I}-\text{I}$	$\text{H}-\text{I}$	$\text{H}-\text{O}-\text{I}$	$\text{H}-\text{O}-\text{I}-\text{I}-\text{I}$	$\text{H}-\text{O}-\overset{\text{H}}{\underset{\text{I}}{\text{I}}}-\text{I}$
H_2O	I_2	HI	HIO	HIO_3	$\text{H}_2\text{I}_2\text{O}$
0.45 a.u.	1.0 a.u.	74.9 a.u.	74.9 a.u.	81.7 a.u.	97.2 a.u.

Figure 5: Lewis structures, molecular formulae, and compound costs determined with starting conditions set for the disproportionation of the six compounds with costs below 100 a.u..

During the exploration, the growing CRN was repeatedly analyzed with PATHFINDER to determine the compound costs of all other compounds found. When starting from I_2 and H_2O , all compounds with a compound cost below 100 a.u. (6 compounds in total) were allowed in unimolecular and bimolecular elementary-step trials in the CRN exploration process. Compounds with a compound cost $100 \text{ a.u.} < w_i < 200 \text{ a.u.}$ were only reacted with each other and with the six cheapest compounds, elementary-step trials with themselves were not permitted in the exploration process. For all compounds with costs above 200 a.u., only trials with the six cheapest compounds were probed to limit the total number of trials.⁶ The rationale behind these choices is that the likeliest encounter of compounds with a high cost is with compounds of low costs. The six compounds with costs below 100 a.u. are shown in Fig. 5, including the starting materials H_2O and I_2 . All compounds with a cost below the one of HIO_3 and including HIO_3 were probed for trials in the exploration with CHEMOTON.

After completion of these trials, the CRN was analyzed with different starting conditions to investigate the reactivity of HIO_3 with H_2O and the resulting products; namely, HIO_3 and H_2O with compound costs set to 1.0 a.u. and 0.45 a.u. H_2O had the same cost assigned as in the PATHFINDER analyses before, the compound cost of HIO_3 equaled the cost of I_2 of the preceding exploration round. Due to the different starting conditions, compound costs were different compared to the analysis with I_2 instead of HIO_3 as starting conditions. Compounds with costs up to 34 a.u. were only combined with H_2O in elementary-step trials as we were solely interested in reactions with H_2O at this point.

The graph of the CRN was build from 3916 of the 4540 found reactions. 624 reactions were not considered, because either the forward or the backward reaction barriers were below 4.5 kJ/mol. Reactions with barriers below this threshold were considered

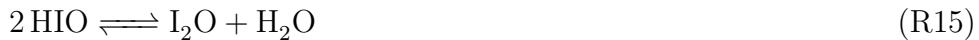
technical failures and therefore not included in the graph. Hence, the resulting graph consisted of 1046 compound nodes and 7832 reaction nodes (LHS nodes and RHS nodes) with 29212 edges.

Among the discovered compounds were hydrogen iodide HI, hypoiodous acid HIO, iodous acid HIO_2 and iodic acid HIO_3 . These cover the oxidation states of iodine from $-\text{I}$ to V . The disproportionation of I_2 to HI and HIO_3 should therefore be included in the CRN as HI and HIO_3 were discovered starting from I_2 and H_2O .



The overall reaction equation of the disproportionation starting from I_2 and H_2O is given in R13. Mechanistic models for the formation of HIO_3 have been discussed in the literature. Early attempts to describe the formation focused on the dissociation of iodine²⁹ and proposed I_2OH , 'invented *ad hoc*',²⁸ as intermediate to react with two equivalents of hypoiodous acid. In a more recent investigation a kinetic model containing ten proposed reactions was fitted successfully to the experimental observations.³⁰ This model proposed I_2OH^- as intermediate to be crucial for fitting the experimental results. Iodate, IO_3^- , was proposed to be formed from two equivalents of IO_2^- . As a caveat, we emphasize that our exploration was performed in the gas phase (see 3). Hence, reactions leading to charged compounds, such as deprotonation reactions, are too high in energy in our setting that precludes dielectric stabilization effects and are therefore not observed in this work.

We chose a kinetic model proposed in the literature^{53,54} as our reference model and slightly modified it. The kinetic reference model for the disproportionation is part of a more complex kinetic model of the Bray–Liebhafsky reaction.^{55,56} The original kinetic model was postulated based on experimental observations and simulation attempts. Our kinetic reference model is represented in R14 to R17. We neglected any dissociation reactions proposed in the original kinetic model in the literature due to the fact that solvent effects were not considered in our exploration. The proposed elementary steps for this kinetic reference model are then:



To illustrate the operation of PATHFINDER, we evaluated the literature path starting

from I_2 and H_2O (left hand side of R14) to HIO_3 (right hand side of R17). This corresponds to the disproportionation of I_2 . Exchanging start and end of the path yields the comproportionation of HI and HIO_3 . We compare the literature path and its length to the shortest path found by PATHFINDER for both directions, shown in Fig. 6, in the following sections. More detailed PATHFINDER output on all paths is given in the SI.

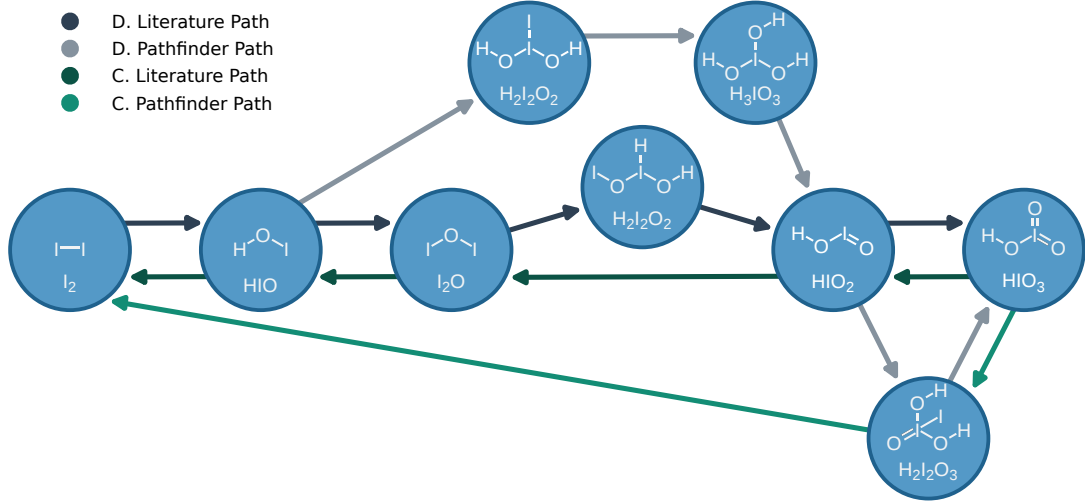


Figure 6: Summary of paths of the disproportionation of I_2 and of the comproportionation of HIO_3 and HI . Compounds are represented as blue nodes with their respective Lewis structure and molecular formula. Reagents and side-products are not shown for clarity. Literature paths derived from experimental observations^{53,54} for the disproportionation (D.) and the comproportionation (C.) are shown with dark gray and dark green arrows, respectively. The PATHFINDER paths for the same start and target compound are shown with light gray and light green arrows.

4.2.1 Disproportionation of I_2

An elementary step is defined as a chemical reaction in which the LHS and the RHS are connected by a single transition state. R14, R15 and R17 were found in the CRN with elementary steps with one transition state (TS). However, R16 turned out to be not an elementary step in our CRN, as there was not one single TS connection the left hand side and right hand side of R16. Instead, the shortest path PATHFINDER proposed to obtain HIO_2 from I_2O under the given disproportionation conditions traversed via compound $H_2I_2O_2$, which has a $HO-I-OH$ motive (compare Fig. 6). The reactions traversed for the formation of compound HIO_2 from I_2O included the highest free activation barrier along the literature path, as can be seen in Fig. 7. The added path lengths are shown in Fig. 8. There were other possible paths with similar lengths.

The total length of the reference path via the intermediate of $\text{H}_2\text{I}_2\text{O}_2$ summed up to 420 a.u., as shown in Fig. 8. Overall, two equivalents of HIO were consumed along this reference path, namely at reaction number two and five of the literature path. As the compound cost of HIO was 75 a.u. (compare Fig. 5) under the stated starting conditions, the total cost of the consumption of the two equivalents of HIO summed up to 150 a.u.. The consumption of two equivalents of HIO therefore was responsible for 36 % of the weight of the path's total length.

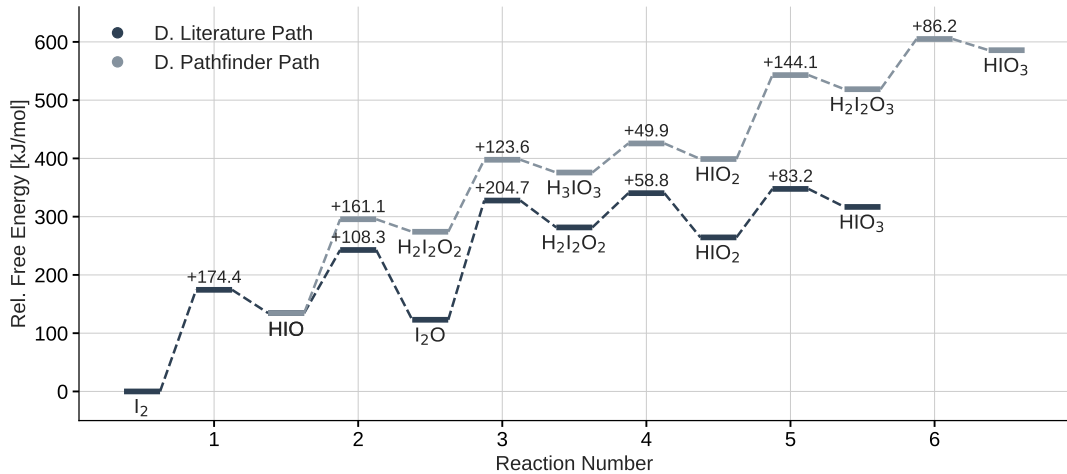


Figure 7: Free energies of the reactions traversed for the shortest disproportionation paths of I_2 under consideration. For each reaction, free activation barriers are added (up) and subtracted (down), respectively. Free activation energies are given above the energy level of the TS of the corresponding reaction.

The shortest path found by PATHFINDER differed at the second reaction step from the reference path. Instead of forming I_2O and consuming one equivalent of HIO, the path traversed via $\text{H}_2\text{I}_2\text{O}_2$, which has a $\text{IO}-\text{I}-\text{OH}$ motive (compare Fig. 6), and H_3IO_3 to form iodous acid HIO_2 . The final steps to iodic acid differed as well, as it was more economical to react with equivalents of the starting compounds I_2 and H_2O compared to HIO in the reference path. This can be seen in Fig. 8, as the reactions five and six of the path by PATHFINDER elongate the total path by a length of 99 a.u., whereas the direct formation via reaction five of the literature path extends the total path by a length of 111 a.u.. Hence, despite the reactions with higher activation barriers (compare Fig. 7), the path from HIO_2 to HIO_3 by PATHFINDER was favorable in terms of path length because of the availability of the required compounds and consequently the lower compound costs. The overall total path length of the PATHFINDER path was 321 a.u. and thereby about 100 a.u. lower than for the literature path. The cost was reduced by avoiding the consumption of two equivalents of HIO which were required in R15 and R17 of the literature path.

The interpretation of a CRN by PATHFINDER depends on the choices made for the

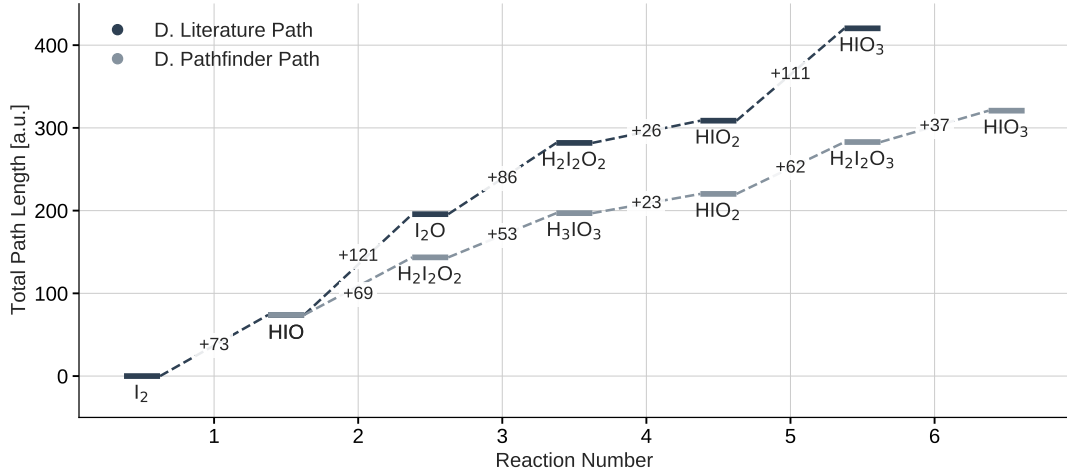


Figure 8: Total path length of the shortest disproportionation paths of I_2 under consideration. For each reaction, the corresponding path length via this reaction is added and the length given.

exploration such as the underlying electronic structure theory, the modeling of the environment (gas phase vs solvation) and the starting conditions for determining the compound costs. Given the limitations of the performed exploration, especially the simplification to exclude any solvation effects, the difference in the reference and PATHFINDER path are not surprising. The compounds along the PATHFINDER path must also be considered with care as some have not been observed experimentally. However, the crucial point of considering the stoichiometric constraints for reactions are clearly covered by the PATHFINDER analysis of a CRN as the reactions of the shortest path for the disproportionation are not consuming any reactants besides the starting materials I_2 and H_2O .

4.2.2 Comproportionation of HIO_3 and HI

For the comproportionation, only HIO_3 and HI were considered as starting compounds. HIO_3 was assigned a compound cost of 1.0 a.u., HI a compound cost of 0.45 a.u.. This corresponded to a probability of 36 % ($e^{-1.0}$) for HIO_3 and 64 % ($e^{-0.45}$) for HI , respectively, being available at the start. As we were analyzing the same CRN as for the disproportionation, the same reactions as discussed before were present. However, a path to form I_2O from HIO_2 was still needed as R16 is not an elementary step in our network. Due to the different starting conditions, the shortest path to form HIO_2 varied from the one found under the disproportionation conditions. PATHFINDER identified a direct formation of I_2O from the reaction of HIO_2 with two equivalents of HIO as the shortest option. The steps found and discussed under disproportionation conditions for R16 were the second best option,

only 0.1 a.u. more expensive.

With the starting conditions set for the comproportionation, the resulting compound cost for HIO was 17 a.u. instead of the 74 a.u. determined under the disproportionation conditions. This illustrates the dependency of the determined compound costs on the chosen starting conditions. The easier formation of HIO was due to the lower reaction barrier of 30.9 kJ/mol from HIO_3 to HIO_2 (compare R17), as shown in Fig. 9, compared to the barrier of 174.4 kJ/mol from I_2 to HIO (compare R14). The highest reaction barrier in the literature path was the formation of HIO from I_2O , reaction three of the path, corresponding to R15. The overall cost of this reference path accumulated to 159 a.u. with reaction three of this path elongating it by 67 a.u..

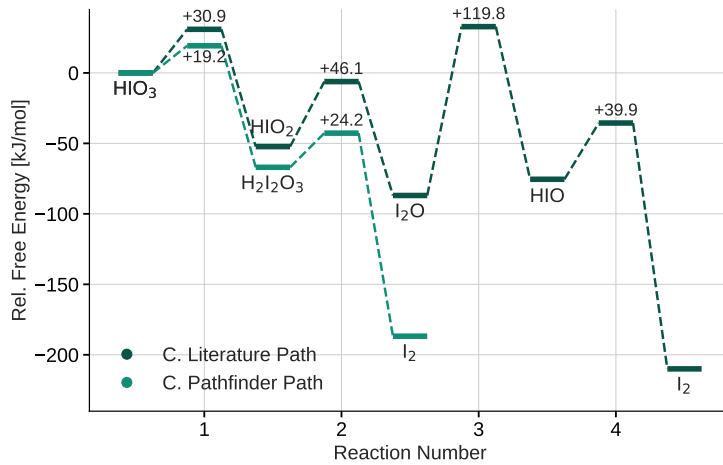


Figure 9: Free energies of the reactions traversed for the comproportionation paths of HIO_3 and HI under consideration. For each reaction, free activation barriers are added (up) and subtracted (down), respectively. Free activation energies are given above the energy level of the TS of the corresponding reaction.

Finding the shortest path to iodine under the given starting conditions according to PATHFINDER required only two reactions, as shown in Fig. 9 and Fig. 10. First, compound $\text{H}_2\text{I}_2\text{O}_3$ (compare Fig. 6) was formed from HIO_3 and HI. This intermediate then reacted again with one equivalent of HI, a cheap starting compound, to form I_2 . The overall length of this path was 24.7 a.u., more than 100 a.u. lower than the literature path. The key feature distinguishing it from the reference path was that only starting compounds were consumed.

As the reference model was based on experimental studies of the disproportionation, its validity for the comproportionation reaction has to be carefully considered. The fact that the shortest path according to PATHFINDER was not overlapping with the literature path indicated that there might be other steps involved. PATHFINDER allows for an almost unbiased approach, with the exception of the choice of the

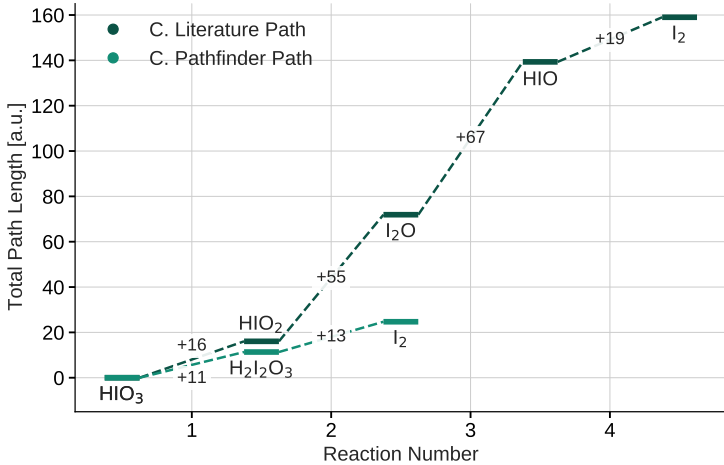


Figure 10: Total path length of the shortest comproportionation paths of HIO_3 and HI under consideration. For each reaction, the corresponding path length via this reaction is added and the length stated.

starting conditions.

5 Conclusions

In this work, we introduced the PATHFINDER algorithm for the fast and efficient analysis of general CRNs represented in a specific graph-based form. In such graphs, kinetic weights are derived from reaction barriers obtained from quantum mechanical reference calculations. They are linked to the likelihood of a reaction in the CRN taking place. To consider the consumption of required reagents during a reaction, compound costs of all compounds in the CRN are determined under given starting conditions. When added to the kinetic weight, both the kinetic information and the reaction conditions of a reaction are encoded in the graph. This avoids explicit kinetic modeling of a CRN with many coupled ordinary differential equations causing exceedingly long simulation times. Instead, the shortest path is found by standard graph algorithms in a cost efficient way. It is then directly possible to query how compounds are formed in terms of a reaction sequence, avoiding the post-processing of a kinetic simulation.

We first demonstrated our algorithm at a synthetic reaction mechanism. Then, we evaluated the disproportionation reaction of I_2 with H_2O . The CRN was generated with CHEMOTON and PATHFINDER where the latter *on-the-fly* ranked the encountered compounds to guide the exploration by exploring only compounds with low costs. This strategy was followed until elementary-step trials of iodic acid with the

six most probable compounds were probed. The obtained CRN was further analyzed with PATHFINDER and paths for disproportionation and comproportionation reactions were compared to paths proposed in the literature. Despite the fact that our exploration only described gas-phase chemistry by construction, interesting observations could be made regarding potentially important neutral species in these reactions.

We emphasize that the graph architecture allows one to analyze the graph in other ways than those considered here. For example, running Monte-Carlo simulations from a starting compound while at each compound node the next reaction node is chosen according to the compound nodes' relative out-flux could help to understand which compounds are formed. Such a procedure would better approximate a full microkinetic modeling attempt on the network. Work along these lines is currently in progress in our laboratory.

Acknowledgments

The authors gratefully acknowledge financial support through ETH grant ETH-44 20-1. This work was presented at the WATOC 2022 conference in July 2022 in Vancouver.

References

- [1] Sameera, W. M. C.; Maeda, S.; Morokuma, K. Computational Catalysis Using the Artificial Force Induced Reaction Method. *Acc. Chem. Res.* **2016**, *49*, 763–773.
- [2] Maeda, S.; Harabuchi, Y. Exploring Paths of Chemical Transformations in Molecular and Periodic Systems: An Approach Utilizing Force. *WIREs Comput Mol Sci* **2021**, *11*, e1538.
- [3] Dewyer, A. L.; Zimmerman, P. M. Finding Reaction Mechanisms, Intuitive or Otherwise. *Org. Biomol. Chem.* **2017**, *15*, 501–504.
- [4] Simm, G. N.; Vaucher, A. C.; Reiher, M. Exploration of Reaction Pathways and Chemical Transformation Networks. *J. Phys. Chem. A* **2019**, *123*, 385–399.
- [5] Unsleber, J. P.; Reiher, M. The Exploration of Chemical Reaction Networks. *Annu. Rev. Phys. Chem.* **2020**, *71*, 121–142.

[6] Steiner, M.; Reiher, M. Autonomous Reaction Network Exploration in Homogeneous and Heterogeneous Catalysis. *Top. Catal.* **2022**, *65*, 6–39.

[7] Baiardi, A.; Grimmel, S. A.; Steiner, M.; Türtscher, P. L.; Unsleber, J. P.; Weymuth, T.; Reiher, M. Expansive Quantum Mechanical Exploration of Chemical Reaction Paths. *Acc. Chem. Res.* **2022**, *55*, 35–43.

[8] Hoops, S.; Sahle, S.; Gauges, R.; Lee, C.; Pahle, J.; Simus, N.; Singhal, M.; Xu, L.; Mendes, P.; Kummer, U. COPASI—a COmplex PAthway SImulator. *Bioinformatics* **2006**, *22*, 3067–3074.

[9] Turányi, T.; Tomlin, A. S. *Analysis of Kinetic Reaction Mechanisms*, 1st ed.; Springer Berlin Heidelberg: Berlin, Heidelberg, 2014.

[10] Proppe, J.; Husch, T.; Simm, G. N.; Reiher, M. Uncertainty quantification for quantum chemical models of complex reaction networks. *Faraday Discuss.* **2016**, *195*, 497–520.

[11] Goodwin, D. G.; Speth, R. L.; Moffat, H. K.; Weber, B. W. Cantera: An Object-oriented Software Toolkit for Chemical Kinetics, Thermodynamics, and Transport Processes. Zenodo, 2018; DOI: 10.5281/zenodo.1174508.

[12] Proppe, J.; Reiher, M. Mechanism Deduction from Noisy Chemical Reaction Networks. *J. Chem. Theory Comput.* **2019**, *15*, 357–370.

[13] Habershon, S. Automated Prediction of Catalytic Mechanism and Rate Law Using Graph-Based Reaction Path Sampling. *J. Chem. Theory Comput.* **2016**, *12*, 1786–1798.

[14] Feinberg, M. *Foundations of Chemical Reaction Network Theory*; Applied Mathematical Sciences; Springer International Publishing: Cham, 2019; Vol. 202; pp 419–440.

[15] Kowalik, M.; Gothard, C. M.; Drews, A. M.; Gothard, N. A.; Weckiewicz, A.; Fuller, P. E.; Grzybowski, B. A.; Bishop, K. J. M. Parallel Optimization of Synthetic Pathways within the Network of Organic Chemistry. *Angew. Chem. Int. Ed.* **2012**, *51*, 7928–7932.

[16] Robertson, C.; Ismail, I.; Habershon, S. Traversing Dense Networks of Elementary Chemical Reactions to Predict Minimum-Energy Reaction Mechanisms. *ChemSystemsChem* **2020**, *2*, e1900047.

[17] Grzybowski, B. A.; Badowski, T.; Molga, K.; Szymkuć, S. Network Search Algorithms and Scoring Functions for Advanced-Level Computerized Synthesis Planning. *WIREs Computational Molecular Science* **2022**, e1630.

[18] Blau, S. M.; Patel, H. D.; Spotte-Smith, E. W. C.; Xie, X.; Dwaraknath, S.; Persson, K. A. A Chemically Consistent Graph Architecture for Massive Reaction Networks Applied to Solid-Electrolyte Interphase Formation. *Chem. Sci.* **2021**, *12*, 4931–4939.

[19] Xie, X.; Clark Spotte-Smith, E. W.; Wen, M.; Patel, H. D.; Blau, S. M.; Persson, K. A. Data-Driven Prediction of Formation Mechanisms of Lithium Ethylene Monocarbonate with an Automated Reaction Network. *J. Am. Chem. Soc.* **2021**, *143*, 13245–13258.

[20] Dijkstra, E. W. A Note on Two Problems in Connexion with Graphs. *Numer. Math.* **1959**, *1*, 269–271.

[21] Yen, J. Y. Finding the K Shortest Loopless Paths in a Network. *Management Science* **1971**, *17*, 712–716.

[22] McDermott, M. J.; Dwaraknath, S. S.; Persson, K. A. A Graph-Based Network for Predicting Chemical Reaction Pathways in Solid-State Materials Synthesis. *Nat. Commun.* **2021**, *12*, 3097.

[23] Barter, D.; Spotte-Smith, E. W. C.; Redkar, N. S.; Dwaraknath, S.; Persson, K. A.; Blau, S. M. Predictive Stochastic Analysis of Massive Filter-Based Electrochemical Reaction Networks. *ChemRxiv* **2022**, DOI: 10.26434/chemrxiv-2021-c2gp3-v2.

[24] Spotte-Smith, E. W. C.; Kam, R. L.; Barter, D.; Xie, X.; Hou, T.; Dwaraknath, S.; Blau, S. M.; Persson, K. A. Toward a Mechanistic Model of Solid-Electrolyte Interphase Formation and Evolution in Lithium-Ion Batteries. *ACS Energy Lett.* **2022**, *7*, 1446–1453.

[25] Bergeler, M.; Simm, G. N.; Proppe, J.; Reiher, M. Heuristics-Guided Exploration of Reaction Mechanisms. *J. Chem. Theory Comput.* **2015**, *11*, 5712–5722.

[26] Simm, G. N.; Reiher, M. Context-Driven Exploration of Complex Chemical Reaction Networks. *J. Chem. Theory Comput.* **2017**, *13*, 6108–6119.

[27] Unsleber, J. P.; Grimmel, S. A.; Reiher, M. Chemoton 2.0: Autonomous Exploration of Chemical Reaction Networks. *J. Chem. Theory Comput.* **2022**, DOI: 10.1021/acs.jctc.2c00193.

[28] Dushman, S. The Rate of the Reaction between Iodic and Hydriodic Acids. *J. Phys. Chem.* **1904**, *8*, 453–482.

[29] Murray, H. D. CXXIII.—The Hydrolysis of Iodine as Measured by the Iodine Electrode. *J. Chem. Soc., Trans.* **1925**, *127*, 882–885.

[30] Sebők-Nagy, K.; Körtvélyesi, T. Kinetics and Mechanism of the Hydrolytic Disproportionation of Iodine. *Int. J. Chem. Kinet.* **2004**, *36*, 596–602.

[31] Truesdale, V. W.; Luther, G. W.; Greenwood, J. E. The Kinetics of Iodine Disproportionation: A System of Parallel Second-Order Reactions Sustained by a Multi-Species Pre-Equilibrium. *Phys. Chem. Chem. Phys.* **2003**, *5*, 3428–3435.

[32] Hagberg, A. A.; Schult, D. A.; Swart, P. J. Exploring Network Structure, Dynamics, and Function Using NetworkX. Proceedings of the 7th Python in Science Conference (SciPy2008). Pasadena, CA USA, 2008.

[33] Bensberg, M.; Grimmel, S. A.; Simm, G. N.; Sobez, J.-G.; Steiner, M.; Türtscher, P. L.; Unsleber, J. P.; Weymuth, T.; Reiher, M. Qcscine/Chemoton: Release 2.0.0. Zenodo, 2022; DOI: 10.5281/zenodo.6695584.

[34] Bensberg, M.; Brandino, G. P.; Can, Y.; Del, M.; Grimmel, S. A.; Mesiti, M.; Müller, C. H.; Steiner, M.; Türtscher, P. L.; Unsleber, J. P.; Weberndorfer, M.; Weymuth, T.; Reiher, M. Qcscine/Heron: Release 1.0.0. Zenodo, 2022; DOI: 10.5281/zenodo.7038388.

[35] Bensberg, M.; Grimmel, S. A.; Simm, G. N.; Sobez, J.-G.; Steiner, M.; Türtscher, P. L.; Unsleber, J. P.; Weymuth, T.; Reiher, M. Qcscine/Chemoton: Release. Zenodo, 2022; DOI: 10.5281/zenodo.6695583.

[36] Bensberg, M.; Brandino, G. P.; Can, Y.; Del, M.; Grimmel, S. A.; Mesiti, M.; Müller, C. H.; Steiner, M.; Türtscher, P. L.; Unsleber, J. P.; Weberndorfer, M.; Weymuth, T.; Reiher, M. Qcscine/Heron: Release. Zenodo, 2022; DOI: 10.5281/zenodo.7038387.

[37] SCINE. <https://scine.ethz.ch>, (accessed 2022-05-06).

[38] Bensberg, M.; Grimmel, S. A.; Sobez, J.-G.; Steiner, M.; Unsleber, J. P.; Reiher, M. Qcscine/Database: Release 1.0.0. Zenodo, 2022; DOI: 10.5281/zenodo.6695496.

[39] Bensberg, M.; Brunken, C.; Csizi, K.-S.; Grimmel, S. A.; Gugler, S.; Sobez, J.-G.; Steiner, M.; Türtscher, P. L.; Unsleber, J. P.; Weymuth, T.; Reiher, M. Qcscine/Puffin: Release 1.0.0. Zenodo, 2022; DOI: 10.5281/zenodo.6695462.

[40] Vaucher, A. C.; Reiher, M. Minimum Energy Paths and Transition States by Curve Optimization. *J. Chem. Theory Comput.* **2018**, *14*, 3091–3099.

[41] Brunken, C.; Csizi, K.-S.; Grimmel, S. A.; Gugler, S.; Sobez, J.-G.; Steiner, M.; Türtscher, P. L.; Unsleber, J. P.; Vaucher, A. C.; Weymuth, T.; Reiher, M. qcscine/Readuct: Release 3.0.0. Zenodo, 2021; DOI: 10.5281/zenodo.5782849.

[42] Sobez, J.-G.; Reiher, M. Molassembler: Molecular Graph Construction, Modification, and Conformer Generation for Inorganic and Organic Molecules. *J. Chem. Inf. Model.* **2020**, *60*, 3884–3900.

[43] Sobez, J.-G.; Reiher, M. qcscine/Molassembler: Release 1.1.0. Zenodo, 2021; DOI: 10.5281/zenodo.5782843.

[44] Bosia, F.; Brunken, C.; Csizi, K.-S.; Grimmel, S. A.; Gugler, S.; Haag, M. P.; Heuer, M. A.; Müller, C. H.; Polonius, S.; Simm, G. N.; Sobez, J.-G.; Steiner, M.; Türtscher, P. L.; Unsleber, J. P.; Vaucher, A. C.; Weymuth, T.; Reiher, M. qcscine/Utilities: Release 4.0.0. **2021**, DOI: 10.5281/zenodo.5782808.

[45] TURBOMOLE V7.4.1 2019, a development of University of Karlsruhe and Forschungszentrum Karlsruhe GmbH, 1989-2007, TURBOMOLE GmbH, since 2007; available from <https://www.turbomole.com>. (accessed 2022-05-06).

[46] Perdew, J. P.; Wang, Y. Accurate and Simple Analytic Representation of the Electron-Gas Correlation Energy. *Phys. Rev. B* **1992**, *45*, 13244–13249.

[47] Perdew, J. P.; Burke, K.; Ernzerhof, M. Generalized Gradient Approximation Made Simple. *Phys. Rev. Lett.* **1996**, *77*, 3865–3868.

[48] Peterson, K. A.; Figgen, D.; Goll, E.; Stoll, H.; Dolg, M. Systematically convergent basis sets with relativistic pseudopotentials. II. Small-core pseudopotentials and correlation consistent basis sets for the post-d group 16-18 elements. *J. Chem. Phys.* **2003**, *119*, 11113–11123.

[49] Weigend, F.; Ahlrichs, R. Balanced basis sets of split valence, triple zeta valence and quadruple zeta valence quality for H to Rn: Design and assessment of accuracy. *Phys. Chem. Chem. Phys.* **2005**, *7*, 3297.

[50] Rappoport, D.; Furche, F. Property-optimized Gaussian basis sets for molecular response calculations. *J. Chem. Phys.* **2010**, *133*, 134105.

[51] Grimme, S.; Antony, J.; Ehrlich, S.; Krieg, H. A Consistent and Accurate Ab Initio Parametrization of Density Functional Dispersion Correction (DFT-D) for the 94 Elements H-Pu. *J. Chem. Phys.* **2010**, *132*, 154104.

[52] Wiberg, N.; Wiberg, E.; Holleman, A. F. In *Anorganische Chemie Band 1 Grundlagen und Hauptgruppenelemente*, 103rd ed.; Holleman, A. F., Ed.; De Gruyter: Berlin/Boston, 2016; pp 525–529, DOI: 10.1515/9783110495850-014.

[53] Schmitz, G. Cinétique de la réaction de Bray. *J. Chim. Phys.* **1987**, *84*, 957–965.

[54] Kolar-Anić, L.; Misljenović, D.; Anić, S.; Nicolis, G. Influence of the Reduction of Iodate Ion by Hydrogen Peroxide on the Model of the Bray-Liebhafsky Reaction. *React. Kinet. Catal. Lett.* **1995**, *54*, 35–41.

[55] Bray, W. C.; Liebhafsky, H. A. Reactions Involving Hydrogen Peroxide, Iodine and Iodate Ion. I. Introduction. *J. Am. Chem. Soc.* **1931**, *53*, 38–44.

[56] Liebhafsky, H. A. Reactions Involving Hydrogen Peroxide, Iodine and Iodate Ion. III. The Reduction of Iodate Ion by Hydrogen Peroxide. *J. Am. Chem. Soc.* **1931**, *53*, 896–911.